P H Y S I C A L   R E V I E W   L E T T E R S

Comparative Hydrodynamics of Bacterial Polymorphism

Saverio E. Spagnolie and Eric Lauga

Department of Mechanical and Aerospace Engineering, University of California San Diego,
9500 Gilman Drive, La Jolla, California 92093-0411, USA

Most bacteria swim through fluids by rotating helical flagella which can take one of 12 distinct polymorphic shapes, the most common of which is the normal form used during forward swimming runs. To shed light on the prevalence of the normal form in locomotion, we gather all available experimental measurements of the various polymorphic forms and compute their intrinsic hydrodynamic efficiencies. The normal helical form is found to be the most efficient of the 12 polymorphic forms by a significant margin—a conclusion valid for both the peritrichous and polar flagellar families, and robust to a change in the effective flagellum diameter or length. Hence, although energetic costs of locomotion are small for bacteria, fluid mechanical forces may have played a significant role in the evolution of the flagellum.

Life in all its diversity is ever changing as form meets function, intimately tuned to nature's diverse environments. Bacteria evolved to swim through fluids by rotating a single helical flagellum ("monotrichous," or polar, bacteria), or in the case of such organisms as *Salmonella* and *Escherichia coli*, several rotating helical flagella emanating from their cell membranes ("peritrichous" bacteria). Flagella are assembled through the polymerization of a flagellin protein, and have been met with great interest both in and outside the scientific community due to its astoundingly complex construction [1]. It has been postulated that the flagellar filaments can take only 12 distinct polymorphic forms [2], of which nine have been characterized experimentally [3] [Fig. 1(a)].

The most common helical waveform is the left-handed normal form, used during forward swimming "runs." Upon counterclockwise [CCW (when viewed from the flagellum's distal end)] corotation of the flagella by rotary motors, a flagellar bundle forms behind peritrichous bacteria, driving fluid backward and propelling the cell forward. To change swimming directions these bacteria undergo "tumbling" events. As shown in Figs. 1(b)–1(e), a quick direction reversal to clockwise (CW) motor rotation produces a twisting torque which temporarily transforms the associated flagellum from a left-handed normal form to a right-handed "semicoiled" form, leading to an unwinding of the bundle and a change in cell orientation, followed by a transition to a right-handed "curly" form which persists until the next reversal in motor direction [4]. The other forms are not generally used for locomotion.

Mechanical stresses, such as the twisting and viscous torques present during swimming, are not the only means by which the flagellar shape might shift from one waveform to another. Filaments can also transform reversibly in response to amino acid replacements, chemical or temperature changes, or the addition of alcohols or sugars [5]. Other authors have considered the elastic rigidity of

different polymorphs and its relationship to shape selection [4,6]. The motion of a helical body through a viscous fluid has seen extensive theoretical treatment [7].

In this Letter we present a physical rationalization of the prevalence of the normal polymorphic form in bacterial swimming. We gather all available experimental measurements of the various polymorphic flagellar waveforms [9] along with the 12 theoretical forms [2], and compute the intrinsic hydrodynamic efficiency of each geometry. We show that the normal form is the most hydrodynamically efficient of the 12 forms by a significant margin, a result true for both peritrichous and monotrichous (polar) flagellar families. This conclusion is robust as the flagellum length is varied, or its effective diameter is increased to represent a bundle of flagella. The hydrodynamic
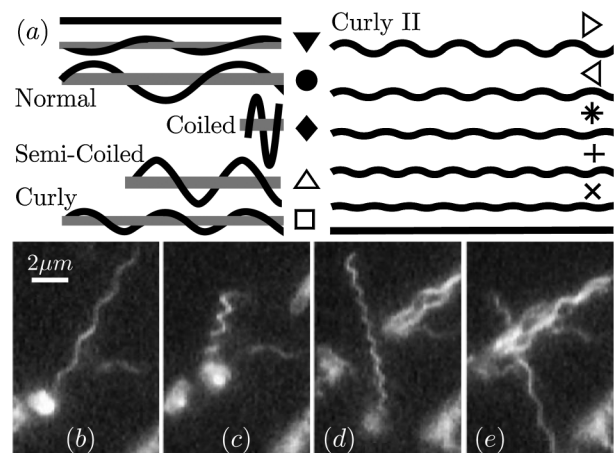

FIG. 1. (a) All 12 theoretical peritrichous polymorphic waveforms, including two straight forms [2]; left-handed (respectively, right-handed) helices are denoted by filled (respectively, empty) symbols. (b) One flagellum of an *E. coli* cell displays a normal waveform; (c) semicoiled; (d) curly; (e) normal again. Adapted with permission from Ref. [8], copyright © 2000, American Society for Microbiology.

optimality of the normal form therefore suggests a role for fluid mechanical forces in the evolution of the flagellum.

We begin with a short description of the hydrodynamics of swimming bacteria. At the exceedingly small length and velocity scales on which bacteria swim, viscous dissipation overwhelms any inertial effects, and the fluid motion is accurately described by the Stokes equations [10]. In this regime, there is a linear relation between the net forces and torques on an immersed flagellum ($\mathbf{F}$, $\mathbf{N}$) and its associated translational and rotational velocities (U, $\boldsymbol{\omega}$) (rigid body motion is assumed). Consider a rotating helix driving a cell body, as is the case for the swimming runs of flagellated bacteria. In this case, the net forces and torques on the rotating flagellum (or flagella) must balance those of the fluid on the body. Assuming that the cell is axisymmetric about $\hat{\mathbf{x}}$ and swims directly along this axis, we write the body's swimming velocity as $\mathbf{U} = U\hat{\mathbf{x}}$ and its rotational velocity as $\boldsymbol{\Omega} = \Omega\hat{\mathbf{x}}$. The corresponding fluid force and torque on the cell body are denoted by $\mathbf{F} = -A_0 U\hat{\mathbf{x}}$ and $\mathbf{N} = -D_0 \Omega\hat{\mathbf{x}}$, respectively. A linear mobility relation for the flagellum may then be written as

$$\begin{pmatrix} \mathcal{A} & \mathcal{B} \\ \mathcal{C} & \mathcal{D} \end{pmatrix} \begin{pmatrix} U \\ \omega \end{pmatrix} = \begin{pmatrix} -A_0 U \\ -D_0 \Omega \end{pmatrix}, \quad (1)$$

where we have written the translational and rotational velocities of each point on the flagellum as $\mathbf{U} = U\hat{\mathbf{x}}$ and $\boldsymbol{\omega} = \omega\hat{\mathbf{x}}$, and neglected hydrodynamic interactions between the flagellum and the body. It can be shown that $\mathcal{C} = \mathcal{B}$ [11]. The cell body counterrotates with respect to the motion of the flagellum, and the rotary motor at the base of the flagellum rotates with angular speed $\Omega_m = \omega - \Omega$.

In order to compare the performance of the various polymorphic forms, a hydrodynamic efficiency $\mathcal{E}^*$ is now defined following Purcell [11]. The power output of the motor, $N\Omega_m$, is compared to the least power required to move the cell body at speed U by any means of propulsion, namely $A_0 U^2$, and so $\mathcal{E}^* = (A_0 U^2)/(N\Omega_m)$. Expressions for U and N in terms of the rotation rate Ω_m may be deduced from Eq. (1), and various approximations valid for the relative length and velocity scales observed in swimming bacteria may be made (for example $\mathcal{B}^2 \ll \mathcal{A}\mathcal{D}$, and $\omega \gg \Omega$) [11]. Allowing for a rescaling of the propeller dimensions, for a given cell body the maximum value of the swimming efficiency can then be found to be given by $\mathcal{E} = \mathcal{B}^2/(4\mathcal{A}\mathcal{D})$; $\mathcal{E}$ is the intrinsic propeller efficiency, and is a function of its shape alone [11,12]. The expression for $\mathcal{E}$ could also be reached using a dimensional approach, as $\mathcal{B}$ indicates the correlation between motor torque and forward swimming, while $\mathcal{A}$ and $\mathcal{D}$ are indicative of the fluid friction [via Eq. (1)]; the ratio above (or factors thereof) is the only such dimensionally proper arrangement.

To determine the intrinsic efficiency $\mathcal{E}$ for each experimentally measured or theoretical waveform, we need only compute the three resistance coefficients $\mathcal{A}$, $\mathcal{B}$, and $\mathcal{D}$. To do so accurately, we perform computations using a nonlocal slender body theory for viscous flows [13]. We consider a single rigid flagellar filament of length L and circular cross-section of radius $\epsilon L r(s)$, where $r(s)$ is dimensionless, $\epsilon \ll 1$ is the aspect ratio of the flagellum ($\epsilon \lesssim 10^{-2}$ for bacteria), and $s \in [0, L]$ is the arclength parameter. For a given translational velocity $U\hat{\mathbf{x}}$ and rotational velocity $\omega\hat{\mathbf{x}}$ about a point $\mathbf{x}_0$, the fluid force $\mathbf{f}(s)$ on the filament is given implicitly via

$$8\pi\mu[U\hat{\mathbf{x}} + \omega\hat{\mathbf{x}} \times (\mathbf{x}(s) - \mathbf{x}_0)]$$
$$= -\boldsymbol{\Lambda}[\mathbf{f}(s)] - \mathbf{K}[\mathbf{f}(s')](s), \quad (2)$$

where μ is the shear viscosity of the fluid, $\mathbf{x}(s)$ denotes the centerline position at a station s, $\boldsymbol{\Lambda}[\mathbf{f}](s) = [c(\mathbf{I} + \hat{\mathbf{s}}\,\hat{\mathbf{s}}) + 2(\mathbf{I} - \hat{\mathbf{s}}\,\hat{\mathbf{s}})]\mathbf{f}(s)$, $\mathbf{K}[\mathbf{f}(s')](s) = (\mathbf{I} + \hat{\mathbf{s}}\,\hat{\mathbf{s}}) \int_0^L \frac{\mathbf{f}(s') - \mathbf{f}(s)}{|s' - s|} ds' + \int_0^L (\frac{\mathbf{I} + \hat{\mathbf{R}}\,\hat{\mathbf{R}}}{|\mathbf{R}(s', s)|} - \frac{\mathbf{I} + \hat{\mathbf{s}}\,\hat{\mathbf{s}}}{|s' - s|})\mathbf{f}(s') ds'$, $c = -\ln(\epsilon^2 e)$, $\mathbf{R}(s', s) = \mathbf{x}(s') - \mathbf{x}(s)$, $\hat{\mathbf{R}} = \mathbf{R}/|\mathbf{R}|$, $\hat{\mathbf{s}}$ is the local unit tangent vector at the point s, and $\hat{\mathbf{s}}\,\hat{\mathbf{s}}$ is a dyadic product [13,14]. Henceforth $\mathbf{x}_0$ is set at the origin, and we have chosen for simplicity $r(s) = \sqrt{4s(L - s)}/L$ to obtain $O(\epsilon^2)$ accuracy. The flagellum diameter d at the midpoint $s = L/2$ is $2\epsilon L$. The waveforms considered are modeled as perfect helices with centerlines $\mathbf{x}(s) = PKs\hat{\mathbf{x}} + (D/2)[\sin(2\pi Ks)\hat{\mathbf{y}} + \cos(2\pi Ks)\hat{\mathbf{z}}]$, with $K = 1/\sqrt{(\pi D)^2 + P^2}$, P the pitch, and D the helical diameter.

We solve Eq. (2) numerically for $\mathbf{f}(s)$ using a Galerkin method [16], in which $\mathbf{f}(s)$ is written as a finite sum of Legendre polynomials, and Eq. (2) is required to hold under inner products against the same basis functions. The first integral in the operator $\mathbf{K}[\mathbf{f}]$ is diagonalized in this space [14]. With $\mathbf{f}(s)$ in hand, we define $F' = \hat{\mathbf{x}} \cdot \int_0^L \mathbf{f}(s) ds$ and $N' = \hat{\mathbf{x}} \cdot \int_0^L (\mathbf{x}(s) - \mathbf{x}_0) \times \mathbf{f}(s) ds$. Then, setting $(U, \omega) = (1, 0)$ we recover $\mathcal{A} = F'$; setting $(U, \omega) = (0, 1)$ we recover $\mathcal{B} = F'$ and $\mathcal{D} = N'$. We estimate that the numerical errors in computing the fluid flow and efficiency calculations for a specified geometry are below 0.1% of the reported values.
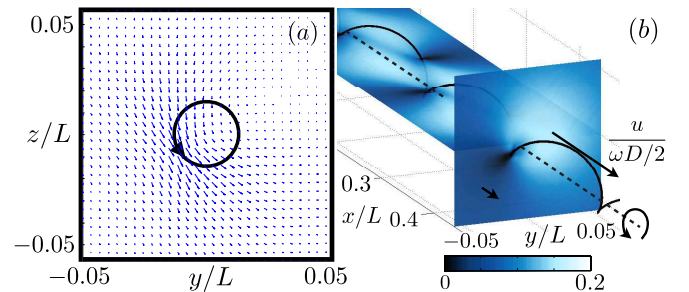

FIG. 2 (color online). A normal waveform undergoes pure CCW rotation about the major helical axis $\hat{\mathbf{x}}$, with $(P, D) = (2.3\ \mu\text{m}, 0.4\ \mu\text{m})$, $L = 10\ \mu\text{m}$, and $d = 20$ nm. (a) Velocity vectors through a cross section at $s = L/2$. A dark arrow indicates both the direction of rotation of the flagellar filament, as well as the location on the filament which intersects the cross-sectional plane. (b) The lengthwise velocity u (the fluid velocity through the cross-sectional plane), normalized by $\omega D/2$.
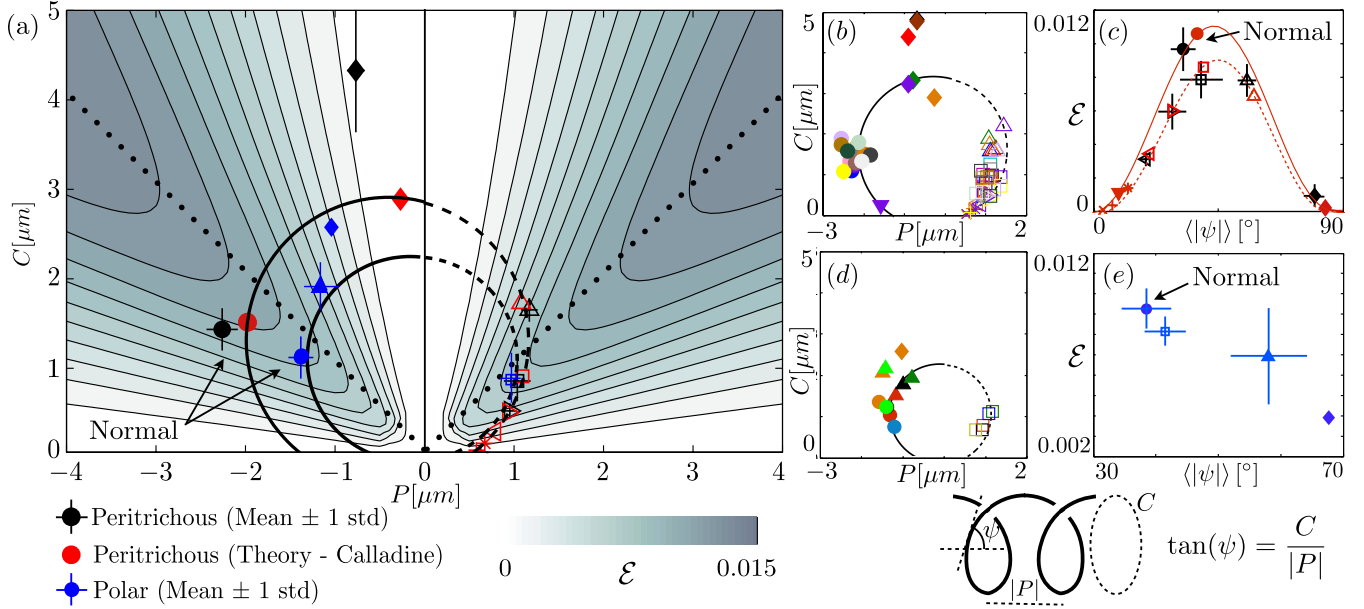
FIG. 3 (color online).   (a) Efficiency contours in the circumference-pitch (C-P) plane ($P < 0$ for left-handed helices, as in diagram), assuming a flagellum diameter (respectively, length) of 20 nm (respectively, 10 μm), combining the information from Figs. 3(b)–3(e). The two large circles distinguish the peritrichous and monotrichous (polar) flagellar families, dashed for $P > 0$. Data points and bars indicate the mean computed efficiency $\pm$ 1 standard deviation for the peritrichous (black online), polar (blue online), and theoretical (red online, from Ref. [2]) waveforms. Dotted lines indicate the curves $C = \pm P$. (b) Waveform geometries from experimental data for the peritrichous flagella (see Tables S1–S4 in the supplemental material [9] and symbols from Fig. 1). Each color represents a different data set. (c) Hydrodynamic efficiencies for each of the peritrichous waveforms as a function of the mean pitch angle, as in (a). Two curves indicate the efficiencies measured continuously along the large circle in the C-P plane in (a); the dashed curve again corresponds to $P > 0$, and the solid curve to $P < 0$. (d),(e) Same as in (b),(c), but for the polar flagellar family [15]. The normal form in each family is the most hydrodynamically efficient of the polymorphic forms by a significant margin.

We show in Fig. 2(a) the velocity field so computed through a cross section of a normal flagellar waveform which is undergoing pure CCW rotation at rate ω. The flow is primarily restricted to the y-z plane, but there is a small lengthwise fluid motion so that fluid is slowly shuttled backward along the axis of rotation. This lengthwise velocity u is displayed in Fig. 2(b), normalized by $\omega D/2$.

For each of the experimentally measured waveforms reported in the literature [9] and the theoretically predicted waveforms [2], we compute the intrinsic efficiency $\mathcal{E}$ using the method described above. In each case we assume a flagellum length $L = 10$ μm and diameter $d = 20$ nm. Figure 3(a) compiles the efficiency results, further detailed in Figs. 3(b)–3(e), overlaid upon efficiency contours in the circumference-pitch (C-P) plane ($C = \pi D$). Different symbols represent the various polymorphic forms (see Fig. 1), and experimental data show averages ± 1 standard deviation. As the filament becomes infinitesimally slender Eq. (2) returns $\mathcal{E} = y^2/(8y^4 + 20y^2 + 8)$, with $y = P/C$. In this limiting case, the efficiency-maximizing geometry has $C = |P|$ (pitch angle $\psi = 45°$), indicated in Fig. 3(a) by dotted lines, and $\mathcal{E} = 2.8\%$. However, at the biologically relevant length scales and aspect ratio as studied here, the optimal geometry has $C \approx (7/8)|P|$ (pitch angle $\psi \approx 40°$).

We plot in Fig. 3(b) the geometrical data in the (C-P) plane which allows the different members of the

peritrichous flagellar family to be distinguished [15]. Each color represents a different data set [9]. The mean hydrodynamic efficiencies of flagellar polymorphs in the peritrichous family are shown in Fig. 3(c) as a function of the average helical pitch angle, $\langle \psi \rangle$, for measured and theoretically predicted waveforms (see [9]). The normal form is found to be the most hydrodynamically efficient of the 12 forms by a significant margin (with $\langle \mathcal{E} \rangle = 0.96\%$) over 23% more efficient than the next most efficient forms, the curly and semicoiled waveforms (both used by bacteria during change-of-orientation events [4]). Two curves indicate the efficiencies measured along the large circle in the C-P plane in (a); the larger efficiencies are achieved along this circle when $P < 0$ (left-handed helices).

A different flagellar family can be distinguished by examining the circumference-pitch curve for different measurements, and is shown in Fig. 3(d). These are monotrichous (polar) flagella, assembled from a different flagellin protein than peritrichous flagella, but which follow a similar polymorphic sequence [15]. Similarly to the peritrichous family, the normal form is the most hydrodynamically efficient one [with $\langle \mathcal{E} \rangle = 1.03\%$; Fig. 3(e)], a 25% increase over the next most efficient shape, a right-handed curly waveform.

To address the robustness of our results against geometrical variations, we changed both the flagellum diameter
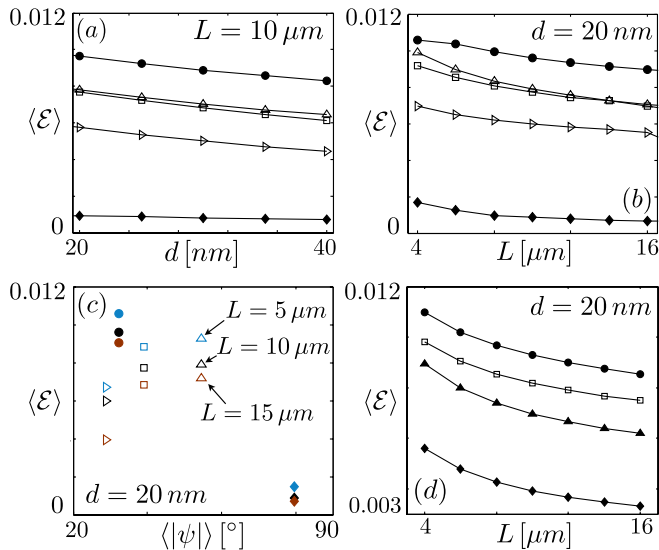
FIG. 4 (color online).   (a) Change in efficiency for the peritrichous family by varying the flagellar diameter from $d = 20$ nm to 40 nm. Greater percentagewise gains in efficiency are obtained for thicker propellers. (b) Varying the flagellar length L. The efficiency ordering remains nearly the same through the biologically relevant length scales. (c) The mean efficiencies of the normal, coiled, semicoiled, curly, and curly II waveforms as functions of the mean pitch angle for three different lengths. (d) Same as (b), but for the polar flagellar family.

and length in our computations. We show in Fig. 4(a) the mean efficiency computed for the peritrichous waveforms as a function of the flagellum diameter, as a model for the increased effective filament size of flagellar bundles. The efficiency decreases steadily as the filament size increases, but the efficiency ordering from Fig. 3(c) is unchanged. The greatest percentage benefit in efficiency when using the normal form is found when the flagellar diameter is large, e.g., for bundles of many flagella. Varying the flagellar length also shows that the efficiency ordering is not modified, as shown in Figs. 4(b) and 4(c), and the greatest percentage increase in the efficiency of the normal form is achieved for longer filaments. We also changed the lengths used in the computations for the polar flagellar family, with the results shown in Fig. 4(d), again showing no change in order. The efficiency orderings shown in Figs. 3(c)–3(e) are therefore robust throughout the biologically relevant parameter space.

Finally, we find that less accurate resistive force theories, the most widely used approaches for modeling slender bodies in fluids, do not predict the efficiency ordering found using the full nonlocal hydrodynamics [7,9,17]. Hydrodynamic interactions between different parts of the helical propeller are thus essential in order to conclude on the relative efficiencies of flagellar polymorphs.

In conclusion, by examining all available experimental data on the geometry of bacterial flagella we have found that both peritrichous and polar bacteria employ, among the discrete number of available flagellar shapes, the hydrodynamically optimal polymorph in order to swim in viscous fluids. In contrast to simple estimates showing that locomotion accounts for a negligible portion of a bacterium's metabolic costs [18], our results suggest that fluid mechanical forces may have played a significant role in the evolution of the flagellum.

[1] K. Namba and F. Vonderviszt, Q. Rev. Biophys. **30**, 1 (1997).
[2] S. Asakura, Adv. Biophys. **1**, 99 (1970); C. R. Calladine, J. Mol. Biol. **118**, 457 (1978); K. Hasegawa, I. Yamashita, and K. Namba, Biophys. J. **74**, 569 (1998).
[3] R. Kamiya, S. Asakura, and S. Yamaguchi, Nature (London) **286**, 628 (1980).
[4] H. Berg, Annu. Rev. Biochem. **72**, 19 (2003); N. C. Darnton and H. C. Berg, Biophys. J. **92**, 2230 (2007); N. C. Darnton et al., J. Bacteriol. **189**, 1756 (2007).
[5] E. Leifson, *Atlas of Bacterial Flagellation* (Academic Press, New York and London, 1960); R. Kamiya and S. Asakura, J. Mol. Biol. **106**, 167 (1976); R. M. Macnab and M. K. Ornston, J. Mol. Biol. **112**, 1 (1977); H. Hotani, BioSystems **12**, 325 (1980); H. C. Hyman and S. Trachtenberg, J. Mol. Biol. **220**, 79 (1991); M. Seville, T. Ikeda, and H. Hotani, FEBS Lett. **332**, 260 (1993).
[6] S. Trachtenberg and I. Hammel, J. Struct. Biol. **109**, 18 (1992); Y. Gebremichael, G. S. Ayton, and G. A. Voth, Biophys. J. **91**, 3640 (2006); S. V. Srigiriraju and T. R. Powers, Phys. Rev. E **73**, 011902 (2006).
[7] G. Taylor, Proc. R. Soc. A **211**, 225 (1952); A. T. Chwang and T. Y. Wu, Proc. R. Soc. B **178**, 327 (1971); J. J. L. Higdon, J. Fluid Mech. **90**, 685 (1979); J. Lighthill, J. Eng. Math. **30**, 35 (1996).
[8] L. Turner, W. S. Ryu, and H. C. Berg, J. Bacteriol. **182**, 2793 (2000).
[9] See supplemental material at http://link.aps.org/supplemental/10.1103/PhysRevLett.106.058103 for experimental data, references, mean efficiency values, waveform geometries, and resistive force theory predictions.
[10] E. Lauga and T. R. Powers, Rep. Prog. Phys. **72**, 096601 (2009).
[11] E. M. Purcell, Proc. Natl. Acad. Sci. U.S.A. **94**, 11 307 (1997).
[12] S. Chattopadhyay et al., Proc. Natl. Acad. Sci. U.S.A. **103**, 13 712 (2006).
[13] R. E. Johnson, J. Fluid Mech. **99**, 411 (1980).
[14] A.-K. Tornberg and M. J. Shelley, J. Comput. Phys. **196**, 8 (2004).
[15] M. Fujii, S. Shibata, and S.-I. Aizawa, J. Mol. Biol. **379**, 273 (2008).
[16] K. E. Atkinson, *The Numerical Solution of Integral Equations of the Second Kind* (Cambridge University Press, Cambridge, U.K., 1997).
[17] S. Chattopadhyay and X.-L. Wu, Biophys. J. **96**, 2023 (2009).
[18] E. M. Purcell, Am. J. Phys. **45**, 3 (1977).